JOURNAL OF combinatorial CHEMISTRY

Article

Setup for High-Throughput Impedance Screening of Gas-Sensing Materials

U. Simon, D. Sanders, J. Jockel, and T. Brinz

J. Comb. Chem., **2005**, 7 (5), 682-687• DOI: 10.1021/cc0500093 • Publication Date (Web): 02 July 2005

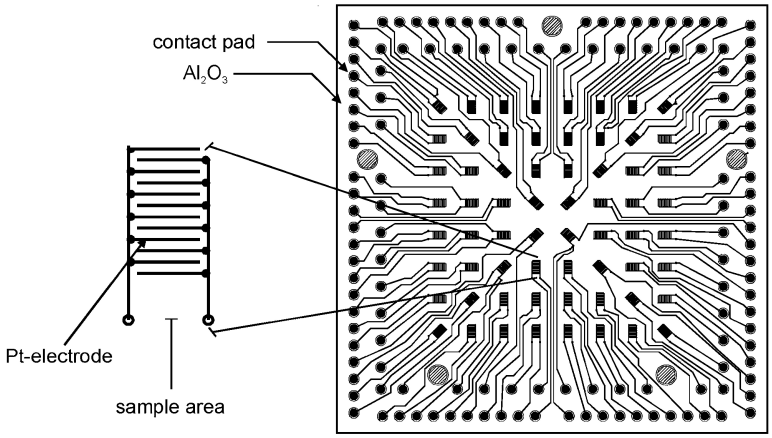

More About This Article

Additional resources and features associated with this article are available within the HTML version:

- Supporting Information
- Links to the 6 articles that cite this article, as of the time of this article download
- Access to high resolution figures
- Links to articles and content related to this article
- Copyright permission to reproduce figures and/or text from this article

View the Full Text HTML

Journal of Combinatorial Chemistry is published by the American Chemical Society.
1155 Sixteenth Street N.W., Washington, DC 20036

Setup for High-Throughput Impedance Screening of Gas-Sensing Materials

U. Simon,*,† D. Sanders,† J. Jockel,‡ and T. Brinz‡

Institute of Inorganic Chemistry, RWTH Aachen University, D-52056 Aachen, and Robert Bosch GmbH, 70839 Gerlingen, Germany

Received January 21, 2005

This paper reports on the setup for a high-throughput impedance measurement system that allows rapid screening of the electrical and dielectrical properties of solid-state sample libraries in variable atmospheres and temperatures. Using multielectrode arrays, most time-consuming steps in the workflow are parallelized. In addition, an approach for automated data evaluation of impedance spectra is presented. For reasons of verification of robust measuring results and reproducibility, screening results of a sample library composed of doped indium(III) oxide as a resistive-type gas-sensing material are discussed on the basis of the determined sensitivities focusing temperature and testing gas gradients.

Introduction

High-throughput experimentation (HTE) is playing an increasing role in material science. The fundamental idea of HTE is the enhancement of sample throughput by acceleration and automation of synthesis and characterization of materials and, subsequently, screening for desired properties.[1,2] The primary fields of application can be found in areas where relationships between structure and properties cannot be predicted precisely, such as in heterogeneous catalysis[2−4] and metal oxide gas-sensing materials.[5−7] This is often due to the fact that the numbers of parameters determining the properties are too large to dissolve their separate effects by sequential investigations. HTE enables the express discovery of new materials with advanced properties as well as provides numerous data available for statistical investigations on structure−property relationships by means of data mining.[8]

In this context, this paper reports on a setup for high-temperature electrical high-throughput screening. Time economization is the crucial point in high-throughput methods. It can be best achieved by parallelization of the most time-consuming steps in the process flow. In the case of high-throughput impedance spectroscopy (HTIS) as an approach in material sciences, these points can be attributed to the preparation of samples and the adjustment of proper measuring conditions. For this reason, the HTIS setup uses 8 × 8 multielectrode arrays, which were recently described by us.[9] By the application of complex impedance spectroscopy (IS) over a broad frequency range, both ion- and electron-conducting materials can be studied. As a further advantage, as compared to DC measurements, electrical properties which are determined by the microstructure of the material, such as grain boundary conductance, interfacial polarization, and polarization of the electrodes, can be analyzed. A gas-mixing unit permits measurements in variable gas atmospheres, making the setup suitable for studies on gas-sensing materials. Gas-sensing materials are the subject of intense research due to the steadily rising need for sensitive and selective sensors for the industrial and private sectors. More and more, gas sensors are used for the control of technical processes, environmental monitoring, health care, domestic applications, and in the automobile sector. We have shown first screening results for gas-sensitive materials based on varying superficially doped tungsten(VI) oxide.[10] For reasons of verification of robust measuring results and reproducibility, a sample library was composed of In(III) oxide as a known resistive gas-sensing material.[11,12] Surface doping resulted in 16 identical samples based on four different dopings. Additives and dopants evidently influence the sensitivity.[13] The results of a test series between 200 and 400 °C in humid synthetic air and under of 25 ppm hydrogen was carried out and will be discussed.

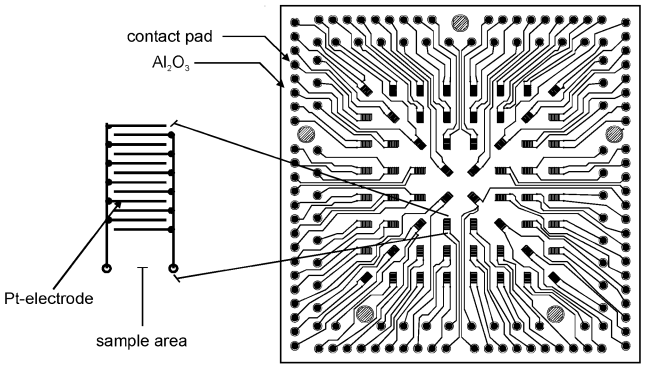

Figure 1. Layout of the 8×8 multielectrode array.

Experimental Setup

Microelectrode Array. Figure 1 outlines the scheme of the microelectrode arrays used. The array is made up of screenprinted platinum leads on an Al_2O_3 ceramic substrate

* To whom correspondence should be addressed. Phone: +49-241-8094644. Fax: +49-241-80 99003. E-mail: ulrich.simon@ac.rwth-aachen.de.

† RWTH Aachen University.

‡ Robert Bosch GmbH.

10.1021/cc0500093 CCC: $30.25
Published on Web 07/02/2005

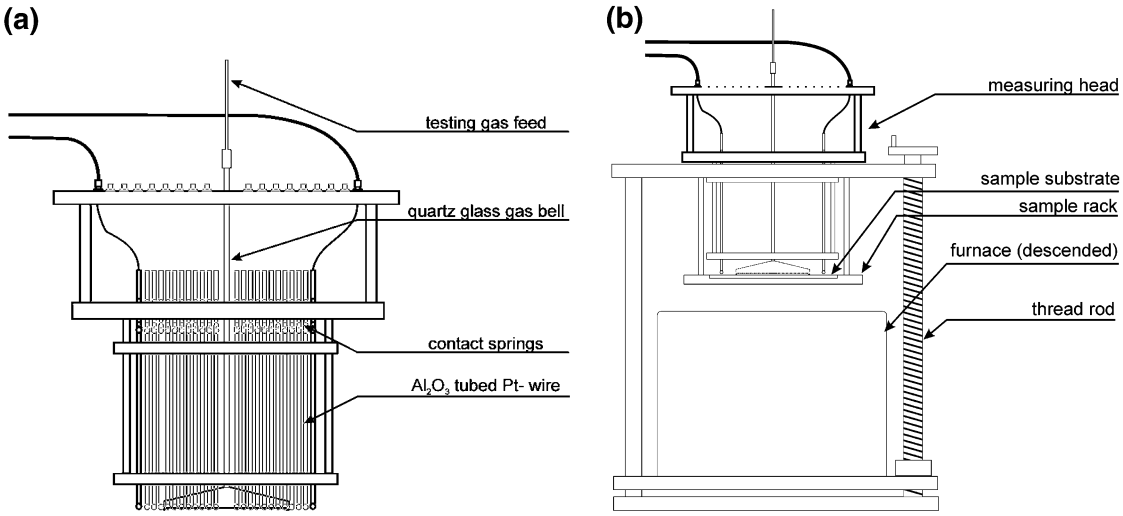

Figure 2. (a) Measuring head and (b) measuring furnace.

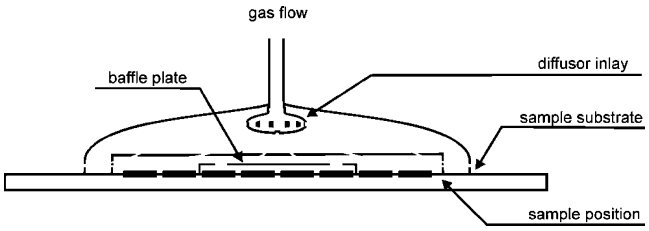

Figure 3. Quartz glass gas bell.

forming 64 interdigital capacitors (IDCs) capable of resistive as well as capacitive measurements. To simplify the contact to the IDCs, a conductor path for each IDC leads to a contact pad outside the array. Numbers according to the $x-y$ position are assigned to the individual IDCs. Detailed specifics of the array can be found in ref 5. The design allows efficient and automated sample preparation and coating. Long-running process steps, such as heating or sample conditioning, proceed in parallel.

Measurement Furnace. To perform impedance measurements, the sample substrates (multielectrode array covered with different materials) are inserted between a sample rack and a mobile measuring head (Figure 2a), where it can be heated by a furnace (Figure 2b).

A mobile measuring head allows thermal decoupling and electrical contact to the electrode array by means of Al_2O_3-surrounded platinum wires whose ends are melted off to form spherical tips. To ensure a constant contact pressure, the wires are depressed at the top by gold-plated contact springs, which are electrically connected to coaxial plugs (SMA). The materials used in the elevated temperature area were chosen as a result of their thermal stability. Load-bearing elements are made of tarnish-proofed elevated temperature stable steel (DIN EN 10095: 1.4828). The guidance for the insulated wires and the sample holder are made of macor, that is, a high-temperature, stress-tolerant, and pore-free ceramic.

In addition, the measuring head holds a quartz glass tube whose lower end forms a bell-shaped cavity (volume ~45 mL) covering the samples on the substrate (Figure 3). Via a diffusor inlay, the bell can be evenly fed with testing gases. A direct laminar flow to the sample substrate is prevented by a 3×3 cm^2 quartz glass plate with four 0.5-mm drilled holes that is placed 4 mm above the substrate. The gas flows out of the bell through crevices formed by 0.8-mm separation distances between the bell and the substrate.

The measuring temperature (room temperature to 800 °C) is achieved by four heating elements in the furnace associated with a thermo-controller (Eurotherm 2416) equipped with a Ni−Cr/Ni thermocouple (Thermocoax) placed below the sample rack. Both gas and temperature distribution on the sample substrate are crucial for the target application and will, therefore, be discussed in the next section.

HTIS Setup. Figure 4 illustrates the HTIS setup. The sample substrate in the measuring furnace (6) is connected to the electrical measuring equipment via the measuring head (5). A set of gas flow controllers (model 1179/2179, MKS Instruments) (4) composes the testing gas of up to eight carrier and testing gases by variation of the flow rate. In addition, carrier gas can be humidified by bubbling through a water reservoir with variable flow to attain a desired degree of humidity. The testing gas is transferred to the quartz bell via stainless steel pipelines (Swagelok, $Ø_{outer}$, 3 mm; length ~1.2 m).

The electrical connecting of the unique samples on the substrate is carried out by two high-frequency capable 3×64 relay matrices (multiplexers) (model KRE-2450-TFCU, MTS-Systemtechnik; frequency range DC, 18 GHz; attenuation DC, 6 GHz max, 0.3 dB)) (3), connecting the SMA plugs on the measuring head and the measuring equipment via coaxial cables (for demonstration reasons, only two cables are shown). Both complex impedance spectroscopy over a frequency range of 10 Hz up to 10^7 Hz (Agilent4192A (1)) and DC measurements (Keithley 2400 (2)) can be carried out.

For automation reasons, a combined control and measuring software was developed to manage the process flow via interfaces (GPIB and RS232, respectively) in all devices. The program supports a basic script language for flexible and nonrestrictive processing of batches.

Experimental Section

For evaluation of the HTIS setup, a sample library was composed by coating a substrate with In(III) oxide. The 16

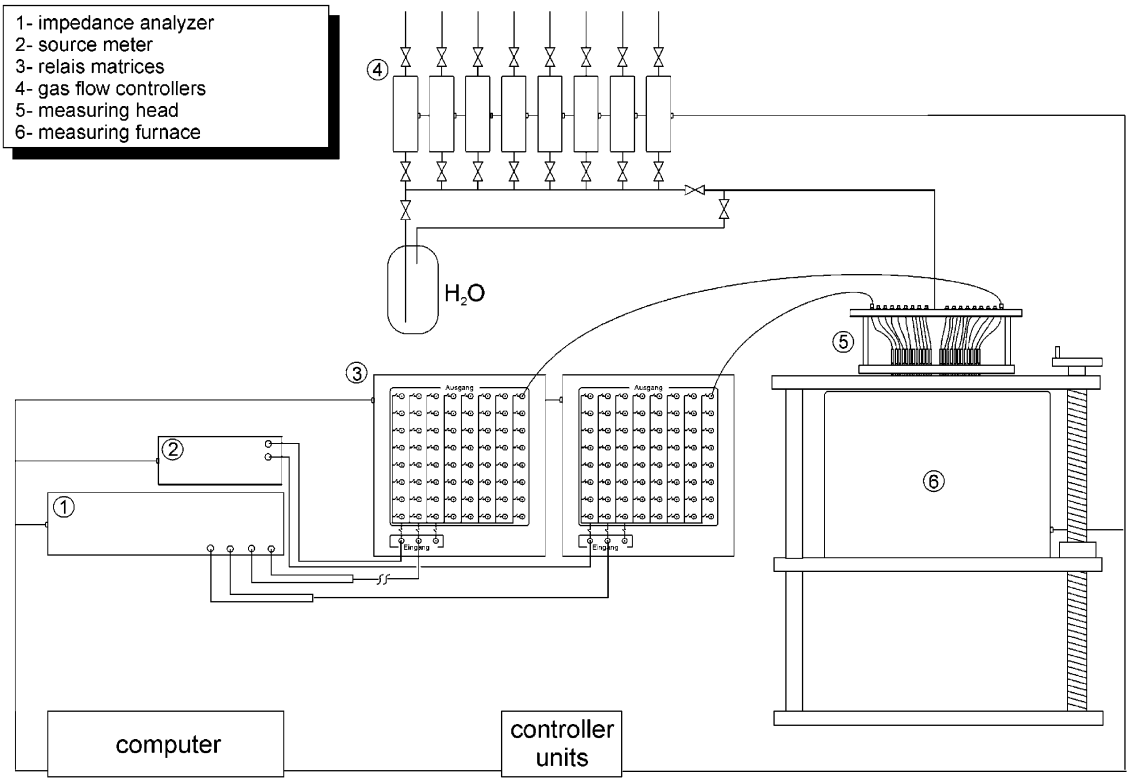

Figure 4. Schematic of the HTIS setup.

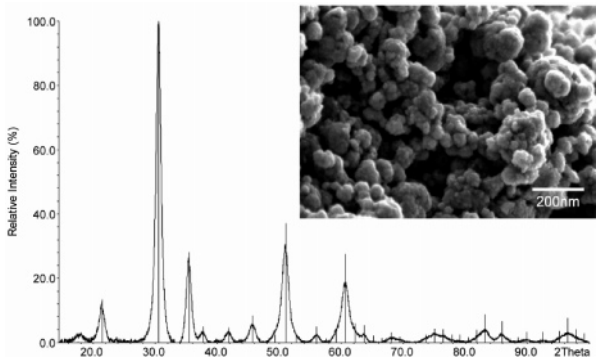

Figure 5. XRD diffraction pattern and scanning electron microscope image of In_2O_3.

samples on a particular quadrant (q) of the substrate were identically impregnated with salt solution of palladium (q1), rhodium (q3), and silver (q4), leaving the second quadrant undoped. In(III) oxide is an n-type semiconductor and was chosen due to its known gas-sensing properties.[11,12] Results from high-throughput impedance spectroscopy screening of the samples in synthetic air and under admixing of hydrogen will be discussed in regard to homogeneity of measurements and sensitivities of identical samples in the following section.

Preparation of the Sample Library. In_2O_3 was obtained by pyrolysis of In(III) acetate at 350 °C. Cubic (206) In_2O_3[14] was obtained by heating the acetate in a crucible for 6 h and characterized by X-ray diffraction (Figure 5). The particle diameters determined by scanning electron microscope (SEM, Figure 5) were in the range of 40−150 nm.

The milled oxide then was suspended in water (solid contents 0.133%$_{wt}$) and applied to each sample position on the substrate via pipetting (mass(In_2O_3)/position ∼ 260 μg). Drying at room temperature resulted in homogeneous layers

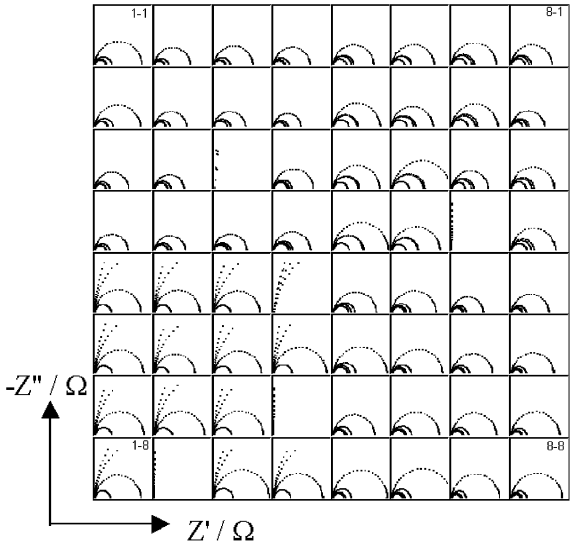

Figure 6. Argand plot of a cooling series (400−250 °C in 50° steps) of the individual samples on a library measured in humid air (r.h. 45%). Full scale of each single diagram corresponds to 250 kΩ. As a result of the scaling, some data are not displayed.

with thicknesses of ∼300 μm. The 0.1%$_{at}$ surface doping was done by wetting impregnation of the particular amount of the respective salt solution and subsequent calcination (5 h at 400 °C in air).

Impedance Screening. Impedance measurements were performed in a temperature range between 400 and 200 °C in humid synthetic air (r.h. 45%) and under admixing of 25 ppm hydrogen at 250, 300, 350, and 400 °C, each with a gas flow of 100 sccm. Figure 6 plots the imaginary −Z″ vs real part Z′ of the complex impedance (Argand plot) of the individual samples. The individual plots represent measure-

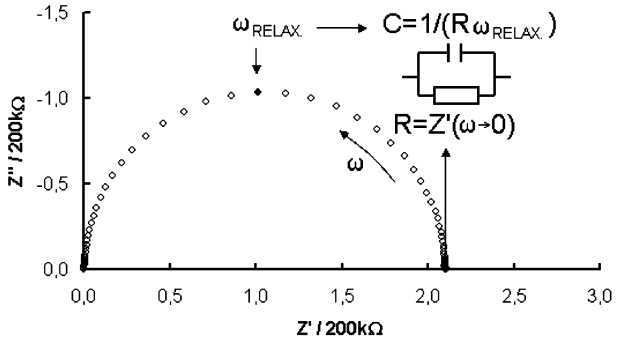

Figure 7. Exemplary Argand plot of position 1−1 at 250 °C and corresponding *R*,*C* circuit equivalent.

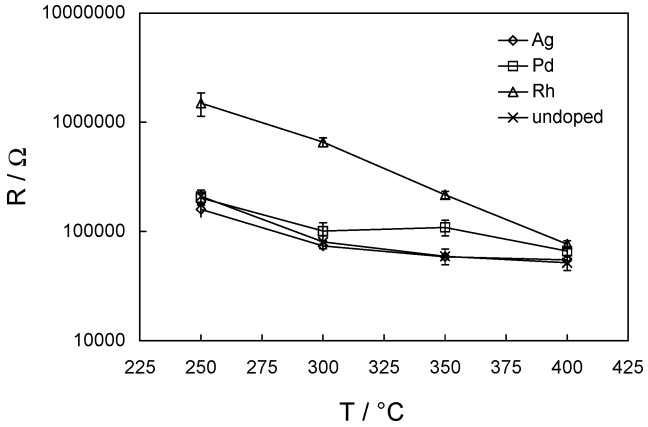

Figure 8. Course of the averaged resistance, *R*, on the measuring temperature for each identical sample in humidified synthetic air. The error bars show the standard deviation.

ments at different temperatures in humid air arranged in the pattern of the samples on the substrate.

The positions 2−8, 3−3, 4−7 and 7−4 show solely capacitive behavior, which can be ascribed either to insufficient contact between the sample and IDC or defect conductor paths on the microelectrode array. All other plots can be described with the impedance function of a parallel *R*,*C* (*r*esistor, *c*apacitor) circuit equivalent as described in Figure 7.

The plot of $-Z''$ versus Z' results in a semicircle. The resistance, *R*, can be determined by extrapolation of the impedance data to the real axis. The capacitance of the sample arises from the frequency of relaxation, ω (radian measure), which corresponds to the frequency of $-Z''_{max}$.

Increasing temperature typically results in smaller semicircles, denoting smaller resistances, as expected for the semiconductor In_2O_3. Figure 8 shows the temperature dependency of the averaged sample resistance for identical samples. For identical samples, a very narrow distibution of resitances can be observed. Doping with Rh strongly enhances the samples' resistance.

An external real-time temperature acquisition on the sample substrate, for instance, by IR-thermography, is not possible due to the inaccessibility of the furnace interior. Therefore, the temperature distribution on the sample positions was deduced indirectly from the individual sample resistances relative to the average resistance for equal samples at different positions on the substrate. With the slope of the tangent, *m*, at the individual temperatures in the plot of log *R* versus *T*, the temperature difference ΔT can be calculated following

$$\Delta T = \frac{m}{(\log \bar{R} - \log R)} \tag{1}$$

where $\bar{R}$ is the average resistance. Figure 9 plots ΔT at different average temperatures arranged according to the samples' position on the substrate.

The temperature differences are in the range of ± 3 K, whereas a gradient on the substrate is not apparent. The deviating behavior of positions 1−5 and 8−2 can be ascribed to an overall different resistivity of the corresponding samples in the whole temperature range due to parasitic effects. Figure 10 displays the Argand plots under humid synthetic air and with admixture of 25 ppm hydrogen at 250 °C.

All samples respond to hydrogen by a decrease in resistance indicated by smaller semicircles, as compared to the measurement in air. At first glance, equally doped samples show similar behavior.

Data Fitting and Evaluation. For automatic determination of the resistance and capacitance values of compounds in circuit equivalents, appropriate fitting software was developed. The fitting algorithm of the software adjusts the impedance function of circuit equivalents to the measured impedance spectra by variation of the particular compounds using difference minimization. The algorithm starts with the adjustment using a circuit equivalent consisting of four serially connected parallel *R*,*C* elements and an inductivity in series. The impedance function used for multiple *R*,*C* elements is given by

$$Z'(\bar{\omega}) = \sum_{i=1}^{n} \cos[\arctan(\bar{\omega} R_i C_i)] \cdot \sqrt{\left(\frac{1}{R_i}\right)^2 + (\bar{\omega} C_i)^{2-1}} \tag{2}$$

$$Z''(\bar{\omega}) = \sum_{i=1}^{n} \left\{ \sin[\arctan(\bar{\omega} R_i C_i)] \cdot \sqrt{\left(\frac{1}{R_i}\right)^2 + (\bar{\omega} C_i)^{2-1}} \right\} + \bar{\omega} L \tag{3}$$

where *L* is the inductance to house lead inductivities and *n* is the number of serial *R*,*C* equivalent circuits

The starting values for *R* and *C* in each *R*,*C* element result from

$$R_{start} = -2Z''_{max} \tag{4}$$

$$C_{start} = \frac{1}{\bar{\omega}_{Z''_{max}} R_{start}} \tag{5}$$

where Z''_{max} and $\omega_{Z''_{max}}$ are determined from the measuring data in the case of the first parallel *R*,*C* circuit equivalent and from the difference spectra of the measuring data and the calculated data in the case of further parallel *R*,*C* elements. A threshold ratio between *R* of the first element, which exhibits the largest resistance, and the resistance values of all other elements are given by the operator for a batch of data to be fitted (the default ratio is 0.1). *R*,*C* elements with a smaller ratio are discarded to reduce the number of fitting parameters and the complexity of the circuit equivalent to a minimum. Note that for all impedance spectra shown

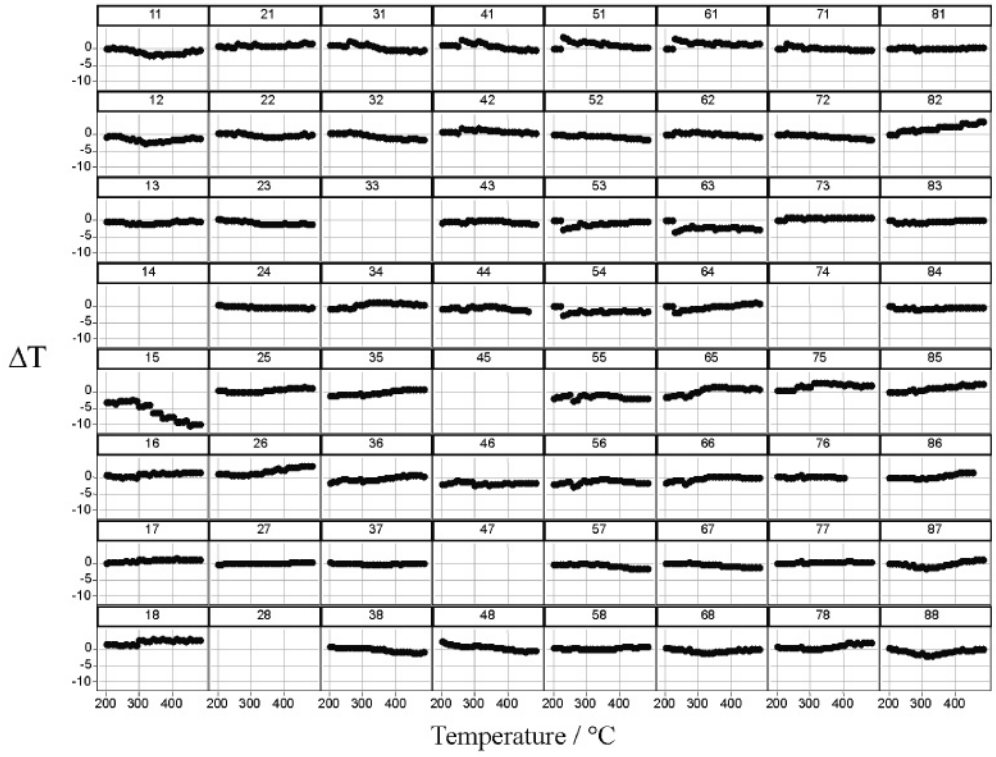

Figure 9. Temperature difference of the sample positions versus the average temperature.

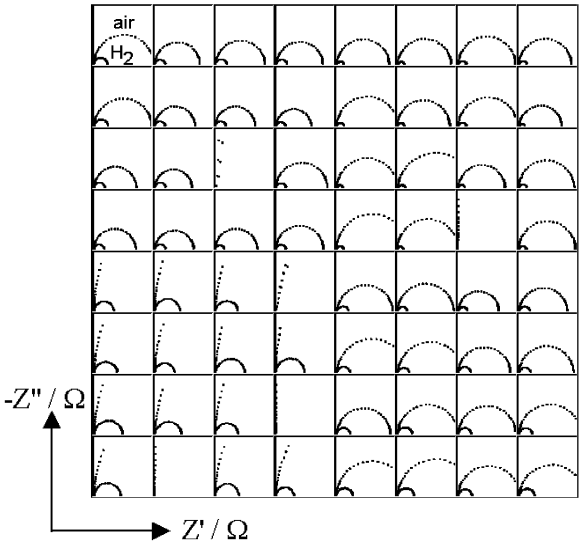

Figure 10. Argand plots of measurements in humid synthetic air (larger semicircles) and under an admixture of 25 ppm hydrogen at 250 °C. Scale of each single diagram is 200 kΩ. As a result of the scaling, some data are not displayed.

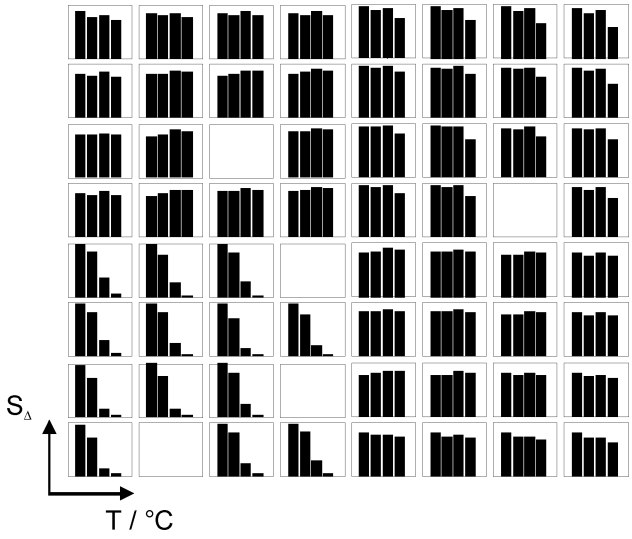

Figure 11. Sensitivity, S_Δ, to hydrogen versus measuring temperature. The height of the bars shows the sensitivity (scale 0−1), while their sequence corresponds to rising temperatures (250−400 °C).

in this work, fitting with a single *R*,*C* element was found to be sufficient.

From the resistances determined by means of the fitting software, the sensitivities of the samples toward hydrogen were calculated using the following equation, according to[10]

$$S_\Delta = \frac{R_{air} - R_{hydrogen}}{R_{air}} \quad (6)$$

Instead of to the commonly used sensitivity *S* as quotient of the resistances in air and under testing gas the scaling toward R_{air} results in values between 0 and 1 and thereby simplifies automated data-mining and -visualization, which is crucial for high-throughput investigations. Figure 11 plots the sensitivities S_Δ toward hydrogen (scale 0 to 1) versus the measuring temperatures (250, 300, 350, and 400 °C).

Almost uniform temperature dependence of the sensitivity is obvious for equally doped samples. Only at 400 °C can a decrease in sensitivity for the samples toward the corners of the substrate be observed, which can be ascribed to reduced H_2 concentration due to partial catalytic conversion. Nevertheless, the testing gas distribution on the sample substrate

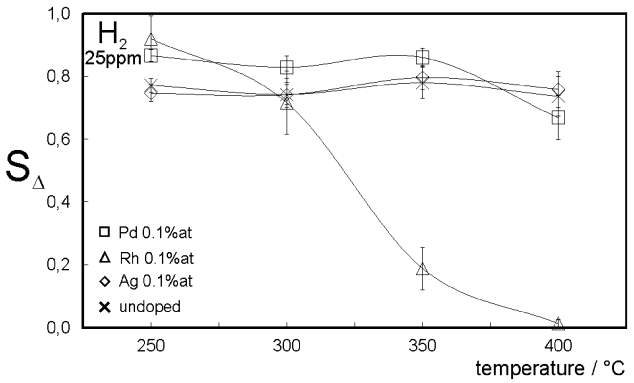

Figure 12. Averaged H_2 sensitivities for identically doped samples together with the standard deviation plotted as error bars.

is sufficiently good to map the sensitivity. Figure 12 points out the H_2 sensitivities for equally doped samples, for example.

The Ag-doped In_2O_3 shows approximately the same trend of sensitivity to temperature as does the undoped sample by passing a weakly pronounced maximum at 350 °C, while S_Δ at all temperatures is well-pronounced. Pd-doped indium oxide exhibits a sensitivity shifted to higher values for temperatures up to 350 °C, followed by a decrease at 400 °C. Doping with Rh leads to the highest sensitivitiy to H_2 at 250 °C, whereas the sensitivity declines with rising temperatures. For these samples, no sensitivity to hydrogen is observed at 400 °C.

Summary

In continuation of our preceding works,[9,10] this paper presents a detailed description of a high-throughput impedance measuring device, which allows high-throughput electrical characterization of solid materials in a wide temperature range and at variable gas atmospheres. Time-economization is achieved by the use of multielectrode arrays supporting fast and parallel processing of the major time-consuming process steps, assisted by complete automation of the measurement and evaluation work flow. A test series on an indium(III) oxide library showed that the temperature distribution over the whole sample plate is homogeneous, with a variation of less than ± 3 K in the investigated temperature range between 200 and 450 °C. Due to combustion of the analyte hydrogen at elevated temperatures, a weak gradient of the testing gas concentration on the substrate was determined, which needs to be taken into account for further data evaluation.

Undoped In_2O_3 exhibits high sensitivity to 25 ppm hydrogen at temperatures between 250 and 400 °C. While superficially doping with Ag 0.1%$_{at}$ has no influence on the sensitivity, elevated sensitivities were observed for samples doped with Pd 0.1%$_{at}$ at temperatures up to 350 °C. Doping with Rh 0.1%$_{at}$ leads to an increase in sensitivity at 250 °C, whereas a decrease occurs at temperatures above 300 °C. Independent of temperature and gas atmosphere, the electrical properties of In_2O_3 can be described by means of a parallel *R,C* circuit equivalent, giving the resistance and capacitance values for the individual measurements.

In addition to the presented application in the discovery of new and advanced gas-sensor materials, a broad range of applications in chemical sensing, catalysis, and microelectronics can benefit from this development.

Acknowledgment. We gratefully acknowledge financial support by the bmb+f under Contract No. FKZ03C0305.

References and Notes

(1) Jandeleit, B.; Schaefer, D. J.; Powers, T. S.; Turner, H. W.; Weinberg, W. H. *Angew. Chem.* **1999**, *111*, 2648−2689.
(2) Schüth, F.; Busch, O.; Hoffmann, C.; Johann, T.; Kiener, C.; Demuth, D.; Klein, J.; Schunk, S.; Strehlau; Zech, T. *Top. Catal.* **2002**, Vol. 21, Nos. 1−3.
(3) Xiang, X.-D.; Schultz, P. G. *Physica C* **1997**, *282−287*, 428−430.
(4) Maier, W. F. *Angew. Chem.* **1999**, *111*, No. 9.
(5) Barsan, N.; Schweizer-Berberich, M.; Göpel, W. *Fresenius' J. Anal. Chem.* **1999**, *365*, 287−304.
(6) Cabot, A.; Vilà, A.; Morante, J. R. *Sens. Actuators, B* **2002**, *84*, 12−20.
(7) Brinzari, V.; Korotcenkov, G.; Golovanov, V. *Thin Solid Films* **2000**, *391*, 167−175.
(8) Sekan, S. *Angew. Chem.* **2001**, *113*, 322−341.
(9) Simon, U.; Sanders, D.; Jockel, J.; Heppel, C.; Brinz, T. *J. Comb. Chem.* **2002**, *4*, 511−515.
(10) Frantzen, A.; Scheidtmann, J.; Frenzer, G.; Maier, W. F.; Jockel, J.; Brinz, T.; Sanders, D.; Simon, U. *Angew. Chem., Int. Ed.* **2004**, *43*, 752−754: *Angew. Chem.* **2004**, *116*, 770−773.
(11) Gurlo, A.; Ivanovskaya, M.; Pfau, A.; Weimar, U.; Göpel, W. *Thin Solid Films* **1997**, *307*, 288−293.
(12) Korotcenkov, G.; Brinzari, V.; Cerneavschi, A.; Ivanov, M.; Cornet, A.; Morante, J.; Cabot, A.; Arbiol, J. *Sens. Actuators, B* **2004**, *98*, 122−129.
(13) Morrison, S. R. *Sens. Actuators* **1987**, *12*, 425−440.
(14) Marezio, M. *Acta Crystallogr.* **1967**, *23*, 1948; *Accra* **1966**, *20*, 723−728.

CC0500093